ChemPubSoc Europe

DOI: 10.1002/chem.201804434

CHEMISTRY A European Journal Full Paper

Nanoparticles |*Hot Paper*|

Black Phosphorus Cytotoxicity Assessments Pitfalls: Advantages and Disadvantages of Metabolic and Morphological Assays

Michaela Fojtů,[a, b] Jan Balvan,[b, c] Martina Raudenská,[b, c] Tomáš Vičar,[b] Daniel Bouša,[a] Zdeněk Sofer,[a] Michal Masařík,[b, c] and Martin Pumera*[a, c]

Abstract: Black phosphorus (BP) belongs to a group of 2D nanomaterials and nowadays attracts constantly increasing attention. Parallel to the growing utilization of BP nanomaterial increase also the requirements for the thorough comprehension of its potential impact on human and animal health. The aim of this study was to compare and discuss five assays commonly used for the cytotoxicity assessments of nanomaterials with a special focus on BP nanoparticles. A comprehensive survey of factors and pitfalls is provided that should be accounted for when assessing their toxicity and pointed to their inconsistency. BP might introduce various levels of interference during toxicity assessments depending on its concentration applied. More importantly, the BP toxicity evaluation was found to be influenced by the nature of assay chosen. These are based on different principles and do not have to assess all the cellular events equally. A commercial assay based on the measurement of protease activity was identified to be the most suitable for the BP toxicity assessment. Further, the benefit of time-lapse quantitative phase imaging for nanomaterial toxicity evaluation was highlighted. Unlike the conventional assessments it provides real-time analysis of the processes accompanying BP administration and enables to understand them deeper and in the context.

Introduction

The explosion of research interest in the field of nanotechnology resulted over the last two decades in the evolution of a spectrum of nanoparticles' applications that are still being broadened. Special group of nanoparticles represent 2D nanomaterials extensively investigated for their applicability in the field of catalysis,[1,2] water pollution,[3] optoelectronic,[2] and biosensor development.[3–5] In last years, these proved to have a significant potential also in biomedical applications, especially in the treatment of cancer. They were successfully used as a non-toxic delivery platform for anticancer drugs.[6,7] Further, 2D nanomaterials showed great promises in the photothermal therapy (PTT), since they are capable of light energy conversion to heat while creating hyperthermia. Besides, they may also be used as a non-toxic photosensitizer for the photodynamic therapy (PDT) that is based on a generation of reactive oxygen species (ROS).[8] Further, 2D nanomaterials were repeatedly reported to inhibit the bacterial growth, to be applicable for the in situ disinfection and described as a promising alternative strategy to combat with the antibiotic resistance of bacteria and biofilms.[9,10] Nanomaterials such as graphene, transition-metal dichalcogenides, or black phosphorus are particles with the third dimension reduced to the sub-nanometer length scale, therefore are termed "2D nanomaterials".[11] Growing application potential of 2D nanomaterials and their increasing incorporation in commercial products are simultaneously placing great demands on their safety for human and animal health, as well as for the environment in general.[12] Therefore, thorough and comprehensive toxicity evaluation should represent crucial decisive milestone preceding the material introduction to the industrial applications.

Black phosphorus (BP) is the most stable among the three phosphorus allotropes. Individual BP atoms create a 2D structure. Since they are in sp^3-hybridization state, phosphorus layers are wrinkled, but still vertically stacked and holding together via weak van der Waals forces.[13] Due to this weak bonding between individual phosphorus layers, bulk BP can be exfoliated into a thin material of few- or single-layer structure.[14] BP evinces a high level of anisotropy. Therefore, changes in the BP structure alter its behaviour and electro-

[a] *Dr. M. Fojtů, Dr. D. Bouša, Prof. Z. Sofer, Prof. M. Pumera*
Department of Inorganic Chemistry
University of Chemistry and Technology Prague
Technická 5, 166 28 Prague 6 (Czech Republic)
E-mail: pumera.research@gmail.com

[b] *Dr. M. Fojtů, Dr. J. Balvan, Dr. M. Raudenská, T. Vičar, Dr. M. Masařík*
Department of Physiology, Faculty of Medicine
Masaryk University, Kamenice 5
625 00 Brno (Czech Republic)

[c] *Dr. J. Balvan, Dr. M. Raudenská, Dr. M. Masařík, Prof. M. Pumera*
Central European Institute of Technology
Brno University of Technology
Technická 3058/10, 616 00 Brno (Czech Republic)

Supporting information and the ORCID identification number(s) for the author(s) of this article can be found under: https://doi.org/10.1002/chem.201804434.

chemical properties.[15] This is favourable for a wide spectrum of diverse applications. Further, after exposure to air or water, it degrades to nontoxic phosphorus intermediates as P_xO_y, thus is considered to be biodegradable.[4,16] Prospective introduction of BP in industrial applications and in the area of biomedicine are holding huge potential. On the other hand, before this happens we should be aware of BP interactions with the environment and with living organisms including human. Therefore, it is absolutely crucial to precisely, quantifiably and reproducibly assess the toxicity of this recently introduced material. Several reports have outlined the difficulties associated with nanoparticle toxicity assessments.[17] In vitro toxicity assessments represent the first key step towards elucidation of the nanomaterial safety profile. These assays are principally based on the evaluation of various molecular events comprising changes in the DNA structure, generation of reactive oxygen species (ROS), disruption of metabolic activity, disruption of cellular membrane, or changes in a cellular morphology. Most of the published studies concerning with the toxicity of nanomaterials use one of the well-established viability assays based on colorimetric and fluorometric detection (Figure 1, Table 1). These assays enable high-throughput toxicity assessment and are considered as a golden standard.[18] Nevertheless, it should be noted that these assays were primarily developed for cytotoxicity assessment of soluble and preferably also colourless compounds. When determining the toxicity of nanomaterials, especially those of 2D shape, their rich surface chemistry should be taken into consideration. Functional groups presented on the particle surface frequently interact with the chemicals used in these conventional assays. Further, since the 2D nanoparticles are usually dark-coloured, the distortion of assessed parameters, for example, absorbance of the solution, may be growing with the increasing concentration of the material. On top of it, peculiarities of each individual toxicity assay should be considered, for example, LDH assay as will be explained below. All these factors may impact the evaluated parameters and consequently, the data may be unintentionally manipulated. This altogether leads either to overestimation, or more dangerously underestimation of the nanomaterial-associated risk. More importantly, it gives rise to some incorrect conclusions regarding the particle biocompatibility, nanotoxicity and safety in general.

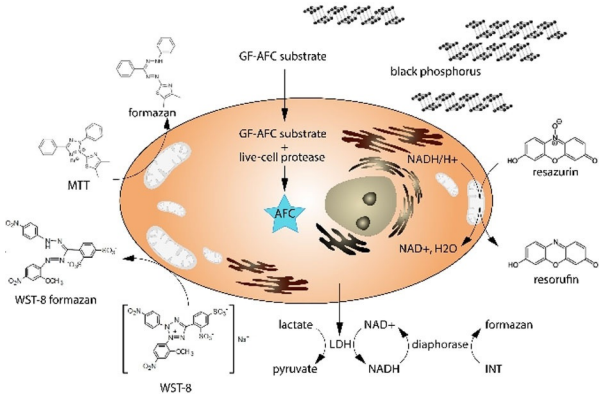

Figure 1. Schematic summary depicting principles of cell viability detection assays used within this study. GF-AFC: glycyl-phenylalanyl-aminofluorocoumarin, LDH: lactate dehydrogenase, INT: 2-*p*-iodophenyl-3-*p*-nitrophenyl-5-phenyl tetrazolium chloride, WST: 8-2-(2-methoxy-4-nitrophenyl)-3-(4-nitrophenyl)-5-(2,4-disulfophenyl)-2*H*-tetrazolium, monosodium salt, MTT: 3-(4,5-dimethyl-2-thiazolyl)-2,5-diphenyl-2*H*-tetrazolium bromide.

Among the most intensively used methods for evaluating cell proliferation and viability belong tetrazolium-salt based assays (MTT, WST, XTT and other) allowing simple, rapid, high-throughput, and inexpensive determination of compound toxicity. MTT, WST-8 and resazurin assay together with non-tetrazolium LDH and Multi-Tox Glo assays are commonly employed for the determination of nanomaterials' toxicity in in vitro toxicological studies.

The assays used in this study were primarily developed for the toxicity assessment of soluble and preferably colourless compounds. Evaluation of nanomaterials' toxicity using these well-established assays should still be possible. However, it

Table 1. Comparison of methods for cellular viability assessment used in this study.

Method	Principle	Advantages	Limitations
MTT	conversion of MTT to water insoluble formazan by enzymes located in cytoplasm and mitochondria	rapid, simple, inexpensive, sensitive, versatile, reliable, appropriate for first rounds of high-throughput studies	can not discriminate between cytotoxic and antiproliferative effects, not working well for assessing compounds altering mitochondrial metabolism
WST-8	enzymatic conversion of WST-8 dye to water-soluble formazan	rapid, simple, sensitive, versatile, reliable, appropriate for the first rounds of high-throughput studies	not working well for assessing compounds altering mitochondrial metabolism
resazurin	reduction of resazurin to resorufin by enzymes located in mitochondria, cytosol and microsomes	rapid, simple, versatile, reliable, appropriate for the first rounds of high-throughput studies	not working well for assessing compounds altering mitochondrial metabolism, sensitive to the presence of proteins in the culture medium
LDH assay	measurement of LDH activity in extracellular medium	rapid, simple evaluation	detects only cell deaths accompanied by LDH leakage, LDH stability and enzymatic activity in supernatants might be affected by several factors
MultiTox	measuring of specific protease activity	rapid, versatile, reliable, allows data normalization	due to the higher cost less appropriate for high-throughput studies

might be not as trivial as it may seem due to their complex physicochemical properties.[19] The MTT salt is widely utilized for the viability assessment. MTT assay is based on colorimetric assessment of dark purple insoluble formazan produced by metabolically active cells by reduction of yellow 3-(-4,5-dimethylthiazol-2-yl)-2,5-diphenyl tetrazolium bromide. For a long time, it was believed that this reduction is taking place mainly in the mitochondria and is catalysed predominantly by mitochondrial succinate dehydrogenase. However, several reports then confirmed that the main site of MTT reduction is in the cytoplasm with the reduced nicotinamide adenine dinucleotide (NAD) coenzyme being the main source of reducing power, followed by ascorbic acid, dihydrolipoic acid, cysteine, tocopherols, and glutathione.[20,21] The resulting insoluble formazan is then solubilized by an organic solvent (e.g., DMSO, isopropanol) prior spectrophotometric measurement. The extent of the MTT reduction is then proportional to the number of viable cells. Several factors may influence the MTT readout, including changes in activity of oxidoreductases, metabolic and energetical fluctuations, or oxidative stress. Therefore, in fact, the MTT assay does not measure the number of viable cells, but rather a complex set of enzyme activities reflecting the level of cellular metabolic state.[22]

Another assay included in this study uses the WST-8 dye belonging to the second generation of tetrazolium salts. These salts are in general cell-membrane impermeable because of their net negative charge hampering them to enter the cell. The reduction site is apparently cell surface, or the transplasma membrane electron transport.[21] The reaction product is water-soluble formazan. Therefore, one reaction step is eliminated compared with the MTT assay since there is no need for using organic solvents. The WST-8 assay results may be influenced by the similar factors as MTT since they principally resemble.[22] Resazurin assay is a fluorescent viability assay based on detecting the cellular metabolic activity. Blue non-fluorescent resazurin is reduced to pink highly fluorescent resorufin by dehydrogenase enzymes located in mitochondria, cytosol and microsomes of metabolically active cells. Therefore, the amount of resorufin produced is proportional to the number of metabolically active cells.[23] Lactate dehydrogenase (LDH) assay is assessing the activity of extracellular LDH released from cells into the extracellular space after irreversible cell damage accompanied by cell membrane injury. Among the advantages of the LDH assay are speed, simplicity and reliability. Moreover, when evaluating this assay, the cells themselves are not taking part in the reaction. Since the LDH is released outside the cell, its activity is quantified from the supernatant.[24] The MultiTox-Glo Multiplex Cytotoxicity Assay™ (further termed "MultiTox") is a commercial kit for measuring a relative number of live and dead cells. This assay measures two protease activities: one is a marker of cell viability, the other determines the number of dead cells. In this study, we used only live cell detection based on measuring cell-permeant peptide substrate that is cleaved by live-cell protease. This generates a fluorescent signal proportional to the number of living cells.[25]

This study provides a deeper insight into limitations of individual viability assays for the toxicity evaluation of BP nanoparticles. Further, flow-cytometry and quantitative phase time-lapse imaging is employed to clarify the differences among individual toxicity assays that are usually disregarded in studies determining the safety of nanomaterials.

Results and Discussion

Synthesis and characterization of black phosphorus

Black phosphorus (BP) was synthesized by high pressure conversion of red phosphorus. The red phosphorus synthesized was exfoliated by share-force milling in DMF.[26] The morphology of BP nanoparticles was investigated by AFM and TEM (Figure 2). The AFM shows the particles lateral size in the range of 100–300 nm with thickness in the range of 5 to 60 nm. The morphology of particles together with height profile are shown in Figure 2a,b. The small size of the particles was also confirmed by TEM which shows the aggregates of nanoplates with size in the range of tenth to few hundred nanometers. The TEM image with SAED and corresponding HR-TEM image are shown on Figure 2c,d.

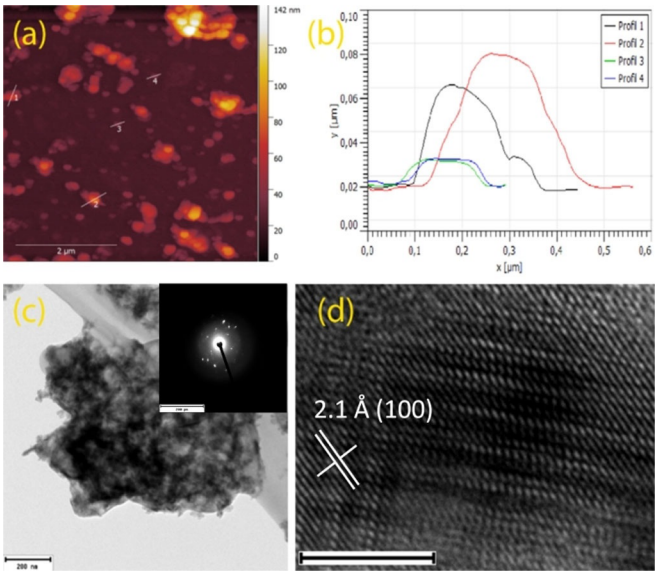

Figure 2. (a) Morphology and (b) height profile of BP nanoparticles, (c) the TEM image and (d) corresponding HR-TEM image (scale bar corresponds to 5 nm).

The X-ray diffraction shows significant broadening of diffraction pattern. The broadening of diffraction pattern corresponds to crystallite size in the range of 10 to 50 nm (Figure 3). The Raman spectroscopy shows the presence of three dominant phonon modes A1g, B2g and A2g characteristic for black phosphorus. The Raman spectra are shown on Figure 3a. The X-ray diffraction shows significant broadening of diffraction pattern (Figure 3b). The crystallite sizes were refined according to the Scherrer formula. The diffraction pattern broadening in (0*k*0) direction correspond to the crystallite size of 33 nm. The broadening originating from in-plane diffraction pattern correspond to the crystallite size in the range of 5–20 nm for indi-

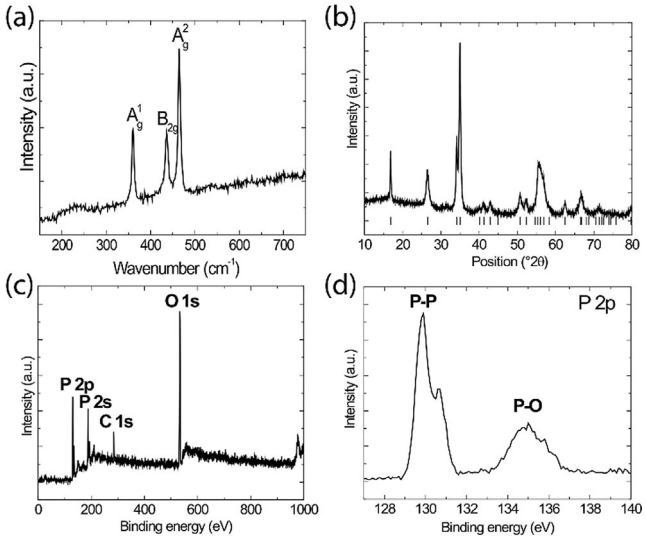

Figure 3. (a) Raman spectra of BP nanoparticles, (b) the X-ray diffractogram, (c) the survey XPS spectra and (d) the high-resolution P 2p spectra.

vidual crystallographic planes. The real particle sizes are bigger since each particle can be composed of several crystallites.[10,27] The chemical composition was verified by X-ray photoelectron spectroscopy. The survey XPS spectra show the presence of phosphorus (P 2p and P 2s characteristic peaks) as well as carbon from surface adsorption and oxygen from surface adsorption and oxygen from surface oxidation (Figure 3c). The oxidation of exfoliated BP in aqueous environment shows two peaks at 130 eV characteristic for P–P bonds in BP and broad P–O bond at 135 eV (see high-resolution XPS spectra of P 2p region on the Figure 3d).

Cell mass calculation

Two cell lines were selected for the BP interference experiments. These were not chosen because of their tissue origin, but due to their different size, since we expect the BP toxicity to be also cell size/mass dependent. A2780 cell line represents the population of cells with smaller size, PC-3 cell culture is a representative of cell line with cells of greater diameter. An interesting phenomenon concerning another 2D nanomaterial, graphene oxide (GO), was formerly observed in a study by Chang et al.[28] They found out that the cytotoxicity of GO particles and reduced graphene oxide (rGO) sheets particle is size-dependent.[28] Similar impact of cellular size/mass on cytotoxicity might be also expected. Therefore, A2780 and PC-3 cells were characterized with respect to their morphology using quantitative phase imaging (Figure 4a, b, respectively).

All analysed parameters (Table 2) were calculated as an average of values acquired by image analysis of 200 cells for each cell line. PC-3 cell mass was more than twice as high than the A2780 cell mass; 574.8 pg and 272.0 pg, respectively. Simultaneously, PC-3 cell area was more than four times bigger than in the case of A2780 cells; 1218.2 μm^2 and 294.8 μm^2, respectively.

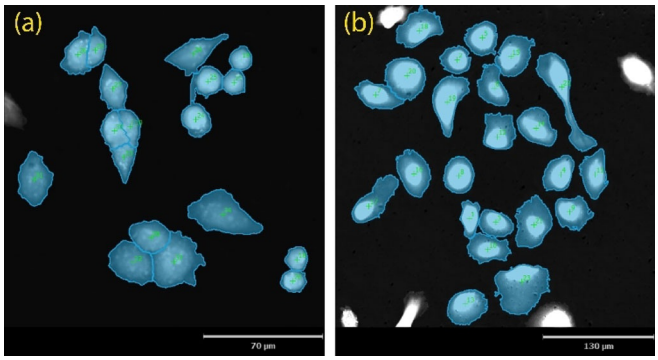

Figure 4. Morphological characterization of (a) A2780 and (b) PC-3 cell line. Example of quantitative phase image segmentation used for further analysis. For each cell line 200 randomly chosen cells were analysed. Average A2780 cell mass was 272.0 ± 144.9, average PC-3 cell mass 574.8 ± 255.1.

Table 2. Morphological characterization of A2780 and PC-3 cell line. Morphological parameters were acquired after quantitative phase image segmentation. For each cell line 200 randomly chosen cells were analyzed.

	Mass [pg]	Area [mm^2]	Perimeter [µm]	Circularity [%]
A2780	272.0 ± 144.9	294.8 ± 242.1	74.1 ± 33.6	67.9 ± 13.0
PC-3	574.8 ± 255.1	1218.2 ± 469.1	161.8 ± 43.2	59.9 ± 14.6

Cytotoxicity assessment of black phosphorus

The cytotoxicity of the BP particles was assessed in two cell lines (Figure 5): human ovarian cancer cell line A2780 and human prostate cancer cell line PC-3. Cell cultures were exposed to BP treatment in a broad concentration range 0–400 $\mu g\,mL^{-1}$ for 24 hours. In this study, we used BP in the form of a colloidal solution in DMF (dimethylformamide). Organic solvents are known for damaging the cellular structures and inducing cytotoxicity.[29] Therefore, to exclude the additional secondary toxicity caused by DMF solvent and misinterpretation of BP toxic effect, DMF was separated from the particles by double centrifugation (14000 rpm, 4 °C, 60 min) followed by washing with sterile water.

First, the toxicity of BP in A2780 cell line was assessed (Figure 5a). In general, the toxicity of BP particles differed significantly depending on the cytotoxicity assay used. The BP half-maximal inhibition concentrations (IC_{50} values) for the ovarian cancer cell line A2780 and BP were 82.5 ± 3.3 $\mu g\,mL^{-1}$ for MTT assay, 61.0 ± 7.8 $\mu g\,mL^{-1}$ for WST-8 assay, 47.7 ± 6.1 $\mu g\,mL^{-1}$ for resazurin assay, 236.9 ± 27.8 $\mu g\,mL^{-1}$ for LDH assay, and 66.7 ± 3.7 for MultiTox-Glo assay (Table 3).

After that, we assessed the toxicity of BP nanomaterial against PC-3 cells (Figure 5b). The toxicity of BP particles again varied according to the assay used. The IC_{50} values assessed by individual assays were determined as follows: $\geq$400 $\mu g\,mL^{-1}$ for MTT assay, 144.1 ± 13.3 $\mu g\,mL^{-1}$ for WST-8 assay, 90.0 ± 1.7 $\mu g\,mL^{-1}$ for resazurin assay, 106.4 ± 12.7 $\mu g\,mL^{-1}$ for LDH assay, and $\geq$400 $\mu g\,mL^{-1}$ for MultiTox assay (Table 3). In general, all methods used confirmed relatively low cytotoxicity of BP

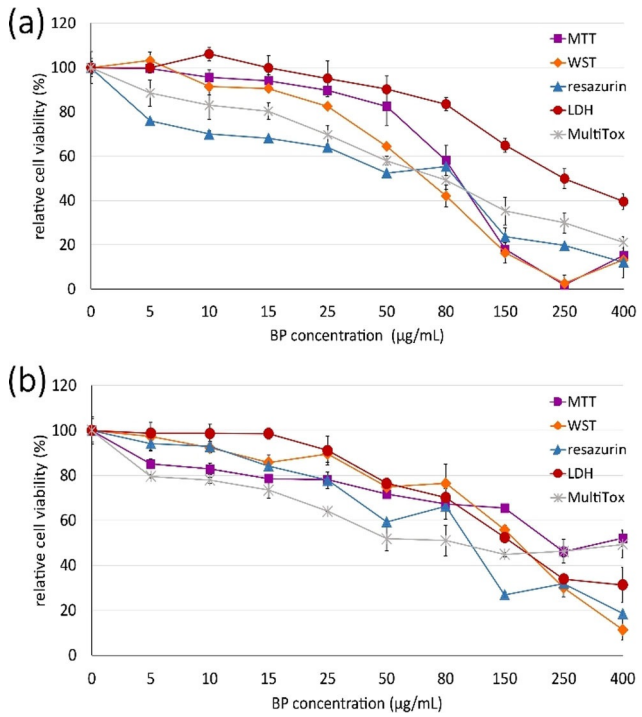

Figure 5. Relative viability of (a) ovarian cancer cell line A2780 and (b) prostate cancer cell line PC-3 after administration of BP assessed by MTT assay (purple), WST-8 assay (orange), resazurin assay (blue), LDH assay (red), and MultiTox-Glo assay (grey). The *x* axis represents BP concentration, range 0–400 μg mL^{-1}, the *y* axis represents relative cell viability. Values are average of three independent measurements, each performed in tetraplicate. Data are displayed as mean ± SD.

Table 3. Comparison of half-maximal inhibition concentration values (IC_{50}) for individual cell lines and assays used for their determination. Data are displayed as mean ± SD.

	IC_{50} A2780 [μg mL^{-1}]	IC_{50} PC-3 [μg mL^{-1}]
MTT	82.5 ± 3.3	≥ 400
WST-8	61.0 ± 7.8	144.1 ± 13.3
resazurin	47.7 ± 6.1	90.0 ± 1.7
LDH assay	236.9 ± 27.8	106.4 ± 12.7
MultiTox	66.7 ± 3.7	≥ 400

for both cell lines up to the concentration of around 15 μg mL^{-1}. Similar toxicity of BP was obtained also in our previous study.[6] For this BP concentration the lowest viability was determined by resazurin assay for both cell lines, 68.1% for A2780 and 84.2% for PC-3 cell line, the highest viability was again for both cell lines assessed by LDH assay, 99.9% for A2780 cell line and 98.6% for PC-3 cell line.

The percentages of viable cells differed significantly among the respective type of viability assessment, various BP concentrations applied and cell lines. Among all assays the biggest difference in determined viability values after application of the same BP concentration was of 48.5% in the case of A2780 cell line (applied BP concentration 150 μg mL^{-1}) and the in the case of PC-3 cell line of about 40.7% (applied BP concentration 400 μg mL^{-1}). In general, all assays except the LDH determined PC-3 cell line to be less sensitive towards BP effect, especially in higher BP concentrations.

In overall, the results obtained from all five cytotoxicity assays differed extensively highlighting both, their high degree of mutual inconsistency when assessing the BP cytotoxicity and apparently also considerable differences among A2780 and PC-3 cell lines concerning their sensitivity towards BP nanoparticles. Recently, Song et al. reported concentration- and time-dependent toxicity of layered BP against fibroblasts using WST-8 kit.[30] After 24 h treatment, they did not detect severe signs of toxicity (cell viability around 82%) up to the concentration of 4 μg mL^{-1} BP. In our study, similar viability (82%) was determined using WST-8 after application of 25 μg mL^{-1} of BP to A2780 cells (the PC-3 cells were even less sensitive to the BP presence). However, not all types of cell death are necessarily accompanied with the reduction of mitochondrial enzymes activity, or LDH leakage out of the cell. This again highlights the need to combine several types of techniques for cytotoxicity measurement. In general, we should be fully aware of that even when analysing other types of nanomaterials, similar degree of inconsistency between individual cytotoxicity assessments and cell lines might be expected. To determine which assay reflects the real cell viability most accurately, Annexin V-FITC/PI staining was subsequently performed.

The background signal of BP particles was determined in the concentration range from 0 to 400 μg mL^{-1} for both cell lines and all the assays except LDH assay (Figure 6). In LDH assay the particles are not presented in the reaction, therefore the BP particle background signal was not defined.

As for the BP particles' interference, the MTT, WST-8, and resazurin assays show similar patterns in BP-induced background signal. In these, an increase of background signal grew proportionally with the BP concentration, starting to be significantly increased from the concentration around 50–80 μg mL^{-1}. This trend might be attributed to their similar principle, for example, measurement of the similar set of enzyme activities. In the MTT assay the background signal comprised from 0–94.2% (A2780) and 0–40.9% (PC-3) of the total signal (peaking for A2780 and PC-3 cells in the BP concentration range of 250 and 400 μg mL^{-1}, respectively), in the WST-8 assay from 0–93.1% (A2780) and 89.6% (PC-3) of signal (peaking for A2780 and PC-3 cells in the BP concentration 250 and 400 μg mL^{-1}, respectively), in resazurin assay from 0–86.8% (A2780) and 83.8% (PC-3) of signal (peaking in the BP concentration 400 μg mL^{-1}). The MultiTox assay, based on the measurement of protease activity, showed mildest fluctuations of background signal through the whole concentration range ranging from 0–31.9% (A2780) and 27.9% (PC-3) of signal (peaking in the BP concentration 400 μg mL^{-1}).

In terms of the BP interference, we may consider LDH and MultiTox as the most suitable methods for determination of BP toxicity: The LDH assay because of the lack of background signal rising from the absence of BP particles. The MultiTox assay was then chosen due to the mildest fluctuations in background signal across the whole concentration range.

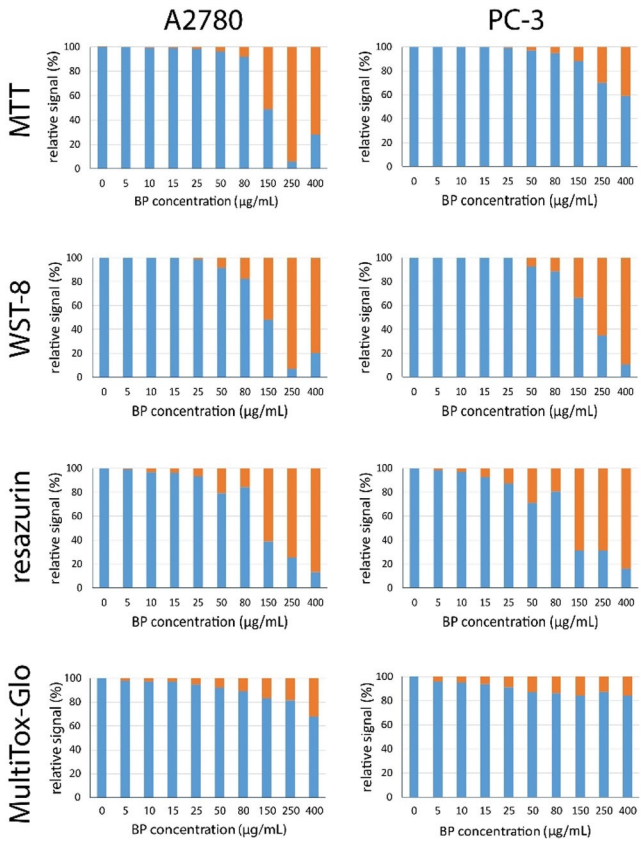

Figure 6. Participation of BP background (orange) on the final signal. BP in the concentration ranging from 0 to 400 μg mL^{-1}. The BP background signal in LDH assay is not stated since the BP particles are not taking part in the cytotoxicity determining reaction. The *x* axis represents BP concentration (μg mL^{-1}), the *y* axis stands for relative signal (%). Values are average of three independent measurements, each performed in tertaplicate.

Annexin V/propidium iodide flow cytometry

The accuracy of toxicity assessments was verified by flow-cytometric analysis using Annexin V-FITC/PI staining. The A2780 and PC-3 cells were treated with 0, 25, 50, 80, and 400 μg mL^{-1} BP. Individual cell stages were identified by the extent of Annexin V expression on the surface of cells and total propidium iodide (PI) uptake using flow cytometry. In the lower BP concentration range (up to 80 μg mL^{-1} BP), the A2780 cells maintained a high viability (more than 80%), however, the highest BP concentration led almost directly to cell death associated with the rupture of plasma membrane (primary, or secondary necrosis): Annexin V+/PI+ cells (Figure S1, Table S1). In the PC-3 cells these processes remained rather low (less than 5.5%) up to the concentration of 80 μg mL^{-1} BP, but unlike the A2780 cells percentage of PI− cells exposing phosphatidylserine (PS) on the outer leaflet of an intact plasma membrane (early apoptotic, or early oncotic): Annexin V+/PI−, was gradually increasing (up to nearly 21% compared to less than 8% in case of A2780 cells). Generally, in the PC-3 cells BP administration primarily induced cell death associated with the exposure of PS in the outer leaflet of the plasma membrane of PI negative cells after administration of lower BP concentrations, the necrotic processes were accompanied to a larger extent of necrotic processes accompanied with the loss of the plasma membrane barrier function occurred only after administration of the highest BP concentration, 400 μg mL^{-1}. Rupture of the cell membrane commonly associated with the necrotic processes was largely occurring after administration of 400 μg mL^{-1} of BP to the smaller A2780 cells (Figure 7). Only 4.73% of the cells remained viable and cell death without plasma membrane rupture stands just for less than 5% of cell deaths, while the necrotic processes were the cause of cell death in almost 66.23% of cases (Table 4). Different results

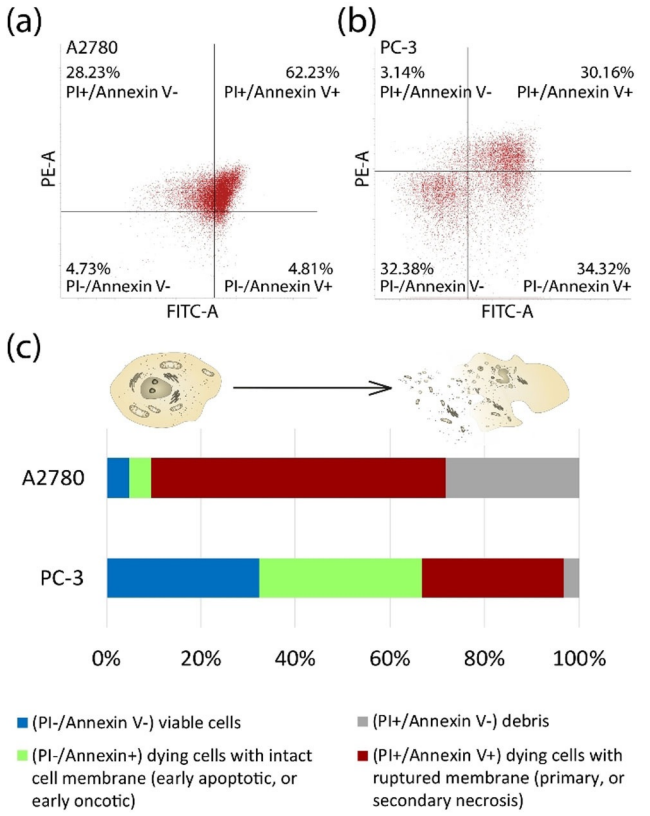

Figure 7. Distribution of viable, early apoptotic, late apoptotic and necrotic (a) A2780 cells and (b) PC-3 cells treated with 400 μg mL^{-1} BP analysed by the extent of Annexin V expression on the surface of cells and total PI uptake using flow cytometry. (c) Diagram showing percentage representation of A2780 and PC-3 cells treated with 400 μg mL^{-1} BP in various states determined using flow cytometry; viable cells (blue), early apoptotic (green), late apoptotic and necrotic stages (red) and cellular debris (grey).

Table 4. Representation of viable, early apoptotic, late apoptotic and necrotic A2780 cells and PC-3 cells treated with 400 μg mL^{-1} BP analysed by the extent of expression of Annexin V on the surface of cells and total PI uptake using flow cytometry expressed in percentages; viable cells (PI−/Annexin V−), early apoptotic (PI−/Annexin V+), late apoptotic and necrotic stages (PI+/Annexin V+) and cellular debris.

	PI−/Annexin−: viable cells	PI−/Annexin+: dying cells with intact membrane	PI+/Annexin+: dying cells with ruptured membrane	PI+/Annexin−: debris
A2780	4.73	4.81	62.23	28.23
PC−3	32.38	34.32	30.16	3.14

were obtained after application of the same BP concentration to PC-3 cells, where more than 32.38% of PC-3 cells remained viable, which is almost seven times more than in the case of the A2780 cell line. The percentage of early apoptotic PC-3 cells was about 34.32% (7-times more than in the A2780 cell line) and the extent of necrotic processes was just 30.16% (twice less than in A2780 cell line). We have shown that BP might induce various level of cellular damage and employ diverse cell death mechanisms depending on the cell line selected and concentration of BP used.

Interestingly, treating A2780 cell with 400 $\mu g\,mL^{-1}$ BP increased the percentage of cellular debris nearly nine times (3.14% for PC-3 cells and 28.23% for A2780 cells). This can be most likely attributed to the presence of apoptotic bodies and most importantly to the disseminated nuclei, organelles and cellular residues released after the cell membrane rupture as a result of intensive necrotic processes. The extent of cellular debris is therefore most evident in A2780 cells after application of the highest BP concentration.

Among the assays mentioned above, the LDH assay at the first glance might seem as the best choice for the toxicity assessment of nanomaterials. The nanomaterials are not taking part in the reaction and therefore, the contribution of unwanted interactions of nanomaterial with the assay's reagents are prevented. Nevertheless, according to our observations, the LDH assay is not optimal for the toxicity determination of BP particles, and this for three reasons: firstly, since the principle of this assessment resides in measuring of released LDH after cell membrane rupture, it is not possible to detect cells undergoing early apoptosis using this assessment. LDH is only released from apoptotic blebs after secondary necrosis occurs.[31] As our results from follow-up flow-cytometry analysis revealed, the proportion of the BP-induced apoptotic cells may extensively differ among cell lines. Therefore, LDH assay may underestimate the real material toxicity by not detecting early apoptotic processes. Secondly, another problem arises if the percentage of material-induced apoptotic cells differs between cell lines extensively as in this case. If the toxicity would be assessed only by LDH assay the cells undergoing apoptosis would be not detected and the toxicity results would be consequently incomparable and misleading. And finally, the level of *LDHA* gene expression might greatly differ between the cell lines. In fact, A2780 and PC-3 cells are not an exception, PC-3 cells were identified to overexpress *LDHA*.[32] This explains why the LDH kit among all other assays was the only one which identified PC-3 cells to be more sensitive to the BP administration, even though according to the flow-cytometry data and the level of induced primary and secondary necrosis it should be the other way around.

The flow-cytometry data revealed a concentration dependent toxicity of BP correspondingly with the data acquired from viability assessment. More specifically, in the case of A2780 cells the percentage of Annexin V+/PI+ cells increased with increasing BP concentration, with the most rapid growth within the concentration range 80–400 $\mu g\,mL^{-1}$. In the PC-3 cell line, the percentage of Annexin V+/PI+ cells also gradually increased with increasing BP concentration, although even more crucial was the presence of early apoptotic processes. Therefore, the Annexin V-FITC/PI staining study helped us to further identify another phenomenon influencing the toxicity assays outputs. After administration of the same BP concentration, cells of different size may have very distinct fate. A limited capability to detect more types of frequently occurring cell death events is one of the reasons why some of the assays might be not suitable for the nanoparticle toxicity evaluation. For example, the LDH assay measures enzymatic activity of LDH released from cells undergoing necrosis after cell membrane rupture. Nevertheless, no LDH is released during early apoptosis[33] and therefore, LDH assay cannot detect it. This statement is supported also by the toxicity data where all viability assays except the LDH assay identified A2780 cells to be more sensitive to the BP effect than PC-3 cells (Table 3). Flow cytometric data were in general in agreement with the MTT and MultiTox assay. However, since MTT evinces a concentration-dependent interference, the MultiTox assay was among other four assays identified to be the most suitable for assessing the BP nanotoxicity. It should be noted, that each of these assays has its own advantages and limitations. Thus, it is absolutely crucial to be aware of pitfalls each of them may be bringing. Therefore, to avoid false positive and false negative results, the combination of at least two well-established methods is highly recommended.

Time-lapse holographic microscopy

To investigate the interaction of BP with cells in more detail, quantitative phase time-lapse imaging was employed. Time-lapse experiments are especially beneficial when analysing material toxicity since, unlike the other "black box end-point methods", enable understanding the accompanied processes not only in context, but also in real time. Time-lapse holographic microscopy is capable of automatic cell segmentation and real-time data quantification (Figure 8). After treating the cells with 80 $\mu g\,mL^{-1}$ BP, amount of accumulated BP was observed. A2780 and PC-3 cells show a very similar trend of BP accumulation with phosphorus average accumulation speed 1.86 and 2.73 percent of cell area covered per minute, respectively (Figure 8a). The PC-3 cells accumulated the BP more rapidly, especially within the first eight hours. The BP accumulation was gradually increasing within the 24 hours in both cell lines. Another evaluated parameter was cell mass (Figure 8b), which in the case of PC-3 cells slightly increased, while A2780 cells rather shrank in the course of time. This decrease in cellular mass is typical for dying cells.[34] Interestingly, the peaks in graphs for the A2780 BP accumulation curve and A2780 cell mass may be observed at the same time. Therefore, A2780 most likely reached a limiting amount of BP accumulated within the cell and their cell membrane ruptured because of induced necrotic processes. No such a phenomenon was observed within the PC-3 cell line. Accumulated BP caused a significant reduction in the motility in both cell lines (Figure 8c). Interestingly, the motility of PC-3 cells was increasing within the first three hours before it started to decrease. This motility drop was most likely caused by a large amount of BP accumu-

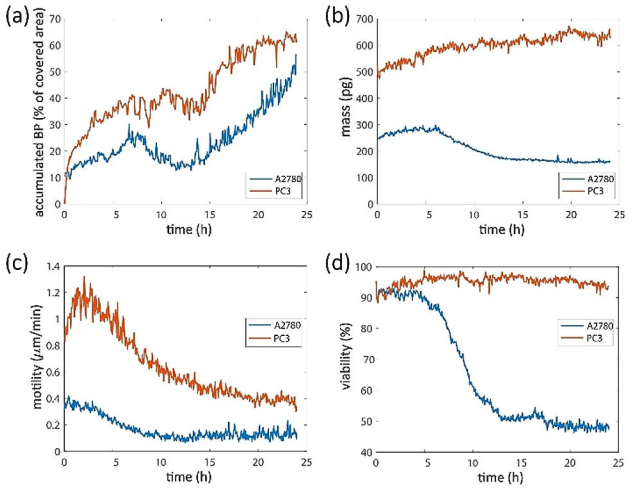

Figure 8. Quantitative phase time-lapse imaging of A2780 and PC-3 cells after administration of 80 μg mL^{-1} BP. Several parameters were evaluated for both cell lines including (a) BP accumulation in A2780 (blue) and PC-3 cells (orange) expressed as a percentage of BP covered area, (b) changes in cell mass, (c) changes in cellular motility, and (d) cell viability. All the evaluated parameters were monitored for 24 hours for each cell line.

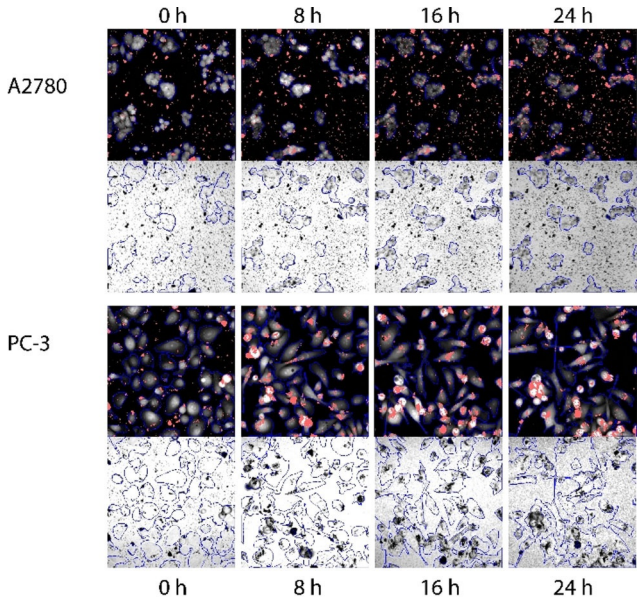

Figure 9. Colocalisation experiment of black phosphorus particles and A2780 and PC-3 cells carried out by merging of phase (upper black images) and amplitude imaging (lower grey images) 0, 8, 16, and 24 hours after BP administration. In phase images (upper black), cells are demarcated by blue line, BP particles are visible as a red dots clustering thru the course of time. In amplitude images (lower grey), cells are demarcated by blue line, BP particles are visible as a black material clustering thru the course of time.

lated within the cell. This oversize cargo then reduced the cell locomotion. On the other hand, the motility of A2780 cells was decreasing right from the first moments after administrating BP and was slowly declining for eight hours. After exceeding initial eight hours after BP administration, the A2780 cell locomotion almost stopped for the rest of the measurement. Since the A2780 cell size is lower than the PC-3 cell size, they are probably also capable only of carrying a lower amount of BP. This may be the cause of their earlier locomotion arrest. Finally, the cell viability was measured within the 24 hours (Figure 8 d). According to the data acquired by quantitative phase imaging administration of 80 μg mL^{-1} BP did not reduce the PC-3 viability significantly while the A2780 viability decreased to 50 %. Interestingly, unlike the A2780 cells, the PC-3 cells seem to absorb BP actively. This can be seen from colocalization experiments and the videos (Figure 9, video S1 and video S2, respectively).

Conclusions

In vitro cytotoxicity assays are common tools for the general safety assessment of nanomaterials as they have a fundamental role in the prediction of their safety for humans, animals and the environment. The wide employment of viability assays in the toxicity evaluation of nanoparticles led in some cases to the ignoring of their biochemical principle, possible interferences and limitations. Here we reported the importance of considering the type of cell death BP induces and the variability of its effect among individual cell lines. A comparison of five assays, which are routinely used for the cytotoxicity evaluation, revealed their inconsistency in the BP toxicity assessment. This was attributed to several phenomena: a different level of background signal BP is inducing in individual assays, different response of distinct cell lines to the BP presence and finally to the nature of each assay which are based on different principles and do not have to assess all the cellular events equally. Finally, a commercial assay which is based on measurement of protease activity, was concluded to be the most suitable assay for determining BP particles' toxicity. It shows the lowest background signal and secondly, the data are in the satisfactory level of agreement with flow-cytometric data and quantitative phase imaging by holographic microscope. These time-lapse experiments obtained by holographic microscope were found to be exceptionally beneficial since these provided an understanding of the accompanied processes in context and in real time. In a summary, our data highlighted the importance of combining several cytotoxicity assessments and the indispensability of determining the type of cell death that the cells are undergoing after administration of nanomaterials. We should be aware of the fact, that BP particles might induce distinct processes in different cell lines. It is absolutely crucial to select the most appropriate method, or to combine it with principally different one, as well as to rigorously evaluate the data these might provide.

Experimental Section

Material preparation

Synthesis of black phosphorus was performed by wrapping the red phosphorus (10 g; 99.999 %, Sigma–Aldrich, Czech Republic) in graphite foil and loading it in the high pressure/high-temperature uniaxial pressing apparatus of 20 mm size. After that, the sample was exhibited to the pressure of 6 GPa and the temperature of

600 °C for 30 min, at a rate of 100 °C min^{-1}. Subsequently, the apparatus was cooled down to the room temperature at the same rate. The graphite foil was removed and resulted black phosphorus was grinded in the agate mortar. Powder containing particles of the size below 0.5 mm was obtained by subsequent sieving the material. Then it was dispersed in DMF by ultrasonication (6.25 mg mL^{-1}; 400 W; 15 min) followed by milling under argon atmosphere in the share force milling apparatus at 17000 rpm in a glass jacketed vessel at 15 °C for 1 h.

Material characterization

X-ray powder diffraction data were collected at room temperature on Bruker D8 Discoverer (Bruker, Germany) powder diffractometer with parafocusing Bragg–Brentano geometry using $Cu_{K\alpha}$ radiation ($\lambda = 0.15418$ nm, $U = 40$ kV, $I = 40$ mA). Data were scanned over the angular range 10–80° (2θ) with a step size of 0.016° (2θ). Data evaluation was performed in the software package EVA. The AFM measurements were carried out on the Ntegra Spectra from NT-MDT. The surface scans were performed in a tapping (semi-contact) mode. Cantilevers with a spring constant of 1.5 kN m^{-1} equipped with a standard silicon tip with curvature radius lower than 10 nm were used for all measurements. For the measurement sample suspension (1 mg mL^{-1}) was drop-casted on freshly cleaved mica substrate. The measurement was performed under ambient condition with a scan rate of 1 Hz and scan line of 512. InVia Raman microscope (Renishaw, England) in backscattering geometry with CCD detector was used for Raman spectroscopy. DPSS laser (532 nm, 50 mW) with applied power of 5 mW and 50× magnification objective was used for the measurement. Instrument calibration was achieved with a silicon reference which gives a peak position at 520 cm^{-1} and a resolution of less than 1 cm^{-1}. The samples were suspended in deionized water (1 mg mL^{-1}) and ultrasonicated for 10 min. The suspension was deposited on a small piece of silicon wafer and dried. High resolution X-ray photoelectron spectroscopy (XPS) was performed using an ESCAProbeP spectrometer (Omicron Nanotechnology Ltd, Germany) with a monochromatic aluminum X-ray radiation source (1486.7 eV). Wide-scan surveys of all elements were performed, with subsequent high-resolution scans of the P 2p peak. Relative sensitivity factors were used to evaluate the carbon-to-oxygen (C/O) ratios from the survey spectra. The samples were placed on a conductive carrier made from a high purity silver bar. An electron gun was used to eliminate sample charging during measurement (1–5 V).

Chemical and biochemical reagents

RPMI-1640 medium, Ham's F12 medium, fetal bovine serum (FBS) (mycoplasma-free), penicillin-streptomycin and trypsin were purchased from PAA Laboratories GmbH (Pashing, Austria). Phosphate buffered saline (PBS) was purchased from Invitrogen Corp. (Carlsbad, CA, USA). Annexin-V-FLUOS Staining Kit was purchased from Roche (Mannheim, Germany). Cell Counting Kit-8 (for WST-8 assay) was obtained from Dojindo Laboratories (Kumamoto, Japan), Multi-Tox-Glo Multiplex Cytotoxicity Assay was purchased from Promega Corporation (Madison, WI, USA), Pierce LDH Cytotoxicity Assay Kit was purchased from Thermo Fischer Scientific (Waltham, MA, USA). Thiazolyl blue tetrazolium bromide (for MTT assay), resazurin sodium salt (for resazurin assay), ethylenediaminetetraacetic acid (EDTA), dimethyl sulfoxide (DMSO) and all other chemicals of ACS purity were purchased from Sigma Aldrich Co. (St. Louis, MO, USA), unless noted otherwise.

Cell line and cell culture

Two human cell lines were used in this study. The human ovarian cell line A2780 was established from a tumour tissue of an untreated patient with ovarian cancer. The cell line was cultivated in RPMI-1640 medium with 10% FBS supplemented with antibiotics (penicillin 100 U mL^{-1} and streptomycin 0.1 mg mL^{-1}). The PC-3 human prostate cell line established from a grade 4 prostatic adenocarcinoma and was cultivated in Ham's medium with 10% FBS supplemented with antibiotics (penicillin 100 U mL^{-1} and streptomycin 0.1 mg mL^{-1}). Cell lines chosen for this experiment were not selected because of some kind of clinical relevance, but rather because of their morphology since A2780 and PC-3 cells differ in size. We expect cellular morphology to be the factor influencing the particle intake. While A2780 cells are small, PC-3 cells are rather larger and possess larger surface area. The cells were grown in the incubator at 37 °C in humidified 5% CO_2 mixture with ambient air. Both cell cultures used in this study were purchased from Health Protection Agency Culture Collections (Salisbury, UK).

Cell mass calculation

Measurement of A2780 and PC-3 cellular size was performed by quantitative phase imaging by Tescan multimodal holographic microscope Q-PHASE. Cells were cultivated in Flow chambers μ-Slide I Lauer Family (Ibidi, Martinsried, Germany). To image enough number of cells in one field of view, objectives Nikon Plan 10/0.30 were chosen. Holograms were captured by CCD camera (XIMEA MR4021 MC-VELETA). The entire image reconstruction and image processing were performed in Q-PHASE control software. From each cell line 200 randomly selected cells were subjected image analysis. Cell dry mass values are derived according to Prescher, Bertozzi, and Wayne[35] from phase, according to Equation (1):

$$m = \frac{\varphi\lambda}{2\pi\alpha} \tag{1}$$

where m represents cell dry mass density (in pg μm^{-2}), φ detected phase (in rad), λ wavelength in μm (0.65 μm in Q-PHASE), and α specific refraction increment, which is ≈ 0.18 μm^3 pg^{-1}. Detected phase values are dependent on two spatially and temporally variable parameters; refractive index and thickness of the sample, according to Equation (2):

$$\varphi = \frac{2\pi(\mathrm{ns} - \mathrm{nm})ts}{\lambda} \tag{2}$$

where n_s and n_m are refractive indexes of sample and medium and t_s is a thickness of the sample (in μm).

Statistical analysis and image processing

Quantitative phase images were analysed with Q-PHASE control software, which includes segmentation based on watershed with region merging, followed by feature extraction (mass, circularity and position) for next analysis.

Preparation of particles for biological analysis

Biological experiments were initiated by sonicating the BP stock solution (6.25 mg mL^{-1} in a DMF) for 15 min in iced bath. The suspension of particles in desired amount was toped up with sterile water up to 500 μL and resulted suspension of particles was centrifuged (14000 rpm, 4 °C, 60 min). After that, the supernatant was removed, and sediment of particles was dispersed again in 1 mL of

sterile water and centrifuged (14000 rpm, 4 °C, 60 min). Particles were used for the further analysis after removing of supernatant and adding the amount of culture media required for analysis.

Cytotoxicity assessment of black phosphorus

MTT viability test: The A2780 cells were seeded on 96-well plate at density 1×10^4 cells/well in RPMI-1640 medium, containing both 10% FBS and 1% penicillin-streptomycin, incubated at 37 °C in humidified 5% CO_2 mixture. The PC-3 cells were seeded on 96-well plate at density 8×10^3 cells/well in Ham's medium, containing both 10% FBS and 1% penicillin-streptomycin, incubated also at 37 °C in humidified 5% CO_2 mixture. After 48 h, the cell culture medium was removed and replaced with a new media containing BP. The BP concentrations ranged from 0 to 400 μg mL^{-1}. After incubating the cells for 24 h 200 μL of medium containing 1 mg mL^{-1} MTT reagent per well was added. Plates were kept in humidified atmosphere at 37 °C for 4 h, wrapped in the aluminium foil. After that, the medium containing MTT was exchanged with 200 μl/well of 99.9% DMSO to dissolve formazan crystals. Then, 25 μL/well of glycine buffer was added to DMSO, gently shaken, and the absorbance was read at a wavelength of 570 nm using Cytation 3 Imaging multimode imaging reader (BioTek Instruments, Winooski, VT, USA). The IC_{50} values were calculated by fitting the data with a logistic function to create sigmoidal dose-response curve. The curve is described by four variables: upper limit, lower limit, skewness of the function, and log IC_{50}. The IC_{50} values define a concentration of compound required to inhibit the cell growth by 50%. All the measurements were performed in tetraplicates.

WST-8 assay: Both the A2780 and the PC-3 cells were seeded at the same density as mentioned above and treated with BP in the same way and for the same time as in the case of MTT viability assay. The WST-8 assay was then performed according the manufacturer's instructions. The absorbance was measured at 450 nm using Cytation 3 Imaging multimode imaging reader (BioTek Instruments, Winooski, VT, USA). The IC_{50} value was defined. All the measurements were performed in tetraplicates.

LDH cytotoxicity assay: Both the A2780 and the PC-3 cells were seeded at the same density as mentioned above and treated with BP in the same way and for the same time as in the case of MTT viability assay. The LDH assay was then performed according the manufacturer's instructions. The absorbance was measured at 490 nm using Cytation 3 Imaging multimode imaging reader (BioTek Instruments, Winooski, VT, USA). The IC_{50} value was defined. All the measurements were performed in tetraplicates.

Resazurin viability assay: Both the A2780 and the PC-3 cells were seeded at the same density as mentioned above and treated with BP in the same way and for the same time as in the case of MTT viability assay. After incubating the cells for 24 h 100 μL of medium containing 0.15 mg mL^{-1} resazurin reagent per well was added. Plates were kept in humidified atmosphere at 37 °C for 4 h, wrapped in the aluminium foil. After that, fluorescence was recorded using 560 nm excitation and 590 nm emission filter using Cytation 3 Imaging multimode imaging reader (BioTek Instruments, Winooski, VT, USA). The IC_{50} value was defined. All the measurements were performed in tetraplicates.

MultiTox-Glo multiplex cytotoxicity assay: Both the A2780 and the PC-3 cells were seeded at the same density as mentioned above and treated with BP in the same way and for the same time as in the case of MTT viability assay. After incubating the cells for 24 h, 50 μL of the GF-AFC reagent per well was added. Plates were wrapped in the aluminium foil, orbitally shaken to ensure homogeneity, and incubated in humidified atmosphere at 37 °C for 2 h. After that, fluorescence was recorded using 400 nm excitation and 505 nm emission filter using Cytation 3 Imaging multimode imaging reader (BioTek Instruments, Winooski, VT, USA). The IC_{50} value was defined. All the measurements were performed in tetraplicates.

Measurement of background signal

The background signal of BP particles in the concentration range from 0 to 400 μg mL^{-1} for particular culture media and individual assays was measured as described in methods above without the presence of cells. The only exception was LDH assay in which the background signal cannot be measured since the BP particles are not taking part in the cytotoxicity determining reaction. In this assay, before the absorbance measurement the cellular supernatant is transferred to a new plate and mixed with a reaction mixture prepared from lyophilized substrate mix and assay buffer supplied by manufacturer.

Annexin V/propidium iodide flow-cytometry

Annexin-V-FLUOS Staining Kit (Roche Applied Science) was used for double-staining the cells with fluorescein isothiocyanate (FITC)/propidium iodide (PI) according to manufacturer's instructions to determine percentages of viable cells, early apoptotic cells, or late apoptotic and necrotic cells following the exposure to assorted concentrations of BP. The cells were seeded on a Petri dish ($d=$ 60 mm) and their number was recalculated in the way the final confluence there corresponds the confluence in a well of 96-well plate in viability assessments. After 48 h, the cells were treated with assorted concentrations of BP (amount of BP corresponding 0, 25, 50, 80, and 400 μg mL^{-1} concentrations during viability assessments). Since the BP nanomaterial sediments on the bottom of the plates and dishes we concluded that the most relevant recalculation will be based on the surface area exposed to BP than on the concentration. The amount of BP applied was recalculated in this way, so it corresponds the BP amount applied in viability assessments. After 24 h treatment, the cells were harvested using a scraper and washed twice with PBS (centrifuged at 2000 rpm for 5 min). Then, they were resuspended in 100 μL of Annexin-V-FLUOS staining solution and incubated for 15 min at a laboratory temperature and in the dark. Cells were resuspended in 500 μL of incubation buffer and Annexin V-FITC binding was detected by flow cytometry (BD FACSVerse, BD Biosciences) using 488 nm excitation and 515 nm bandpass filter for fluorescein detection and filter $>$600 nm for PI detection. The data were analysed using the BD FACSuite software.

Time-lapse holographic microscopy

Quantitative phase imaging of living cells was obtained using Q-PHASE, the coherence-controlled holographic microscope, CCHM (Tescan, Brno, Czech Republic). The microscope setup is based on off-axis holography and incorporates a diffraction grating to allow imaging with both spatially and temporally low-coherent illumination. This leads to a high quality of QPI compared to coherent-illumination digital holographic microscopy (DHM) by suppressing coherence noise (speckles), interferences and diffraction artefacts, while the lateral resolution is enhanced closer to a standard light microscope. The off-axis configuration of the system enables a single shot QPI acquisition.[36]

Quantitative phase time-lapse imaging was initiated immediately after treating the cells with 80 μg mL^{-1} BP. Time-lapse monitoring was performed for 24 h at a frame-rate of 1 frame/3 min. The cells

were observed in flow chambers μ-Slide I Luer Family Cat. No. 80196 (Ibidi, Martinsried, Germany) in RPMI-1640 (for A2780 cells) and Ham's medium (for PC-3 cells). Nikon Plan 10×/0.3 was used for both holographic observations. Interferograms for holography were taken using a CCD camera (XIMEA MR4021MC). The fluorescence mode used a solid-state light source (Lumencor Aura II) and a sCMOS camera (Andor Zyla 5.5, 2560×2160px) was used to capture the images.

The holographic raw data must be numerically reconstructed. The numerical reconstruction is performed by the custom software where the established methods of the fast Fourier-transform and phase unwrapping are implemented. The output from the software is an unwrapped phase image. This image has intrinsic high contrast and can be processed by an available image processing software.

Dry cell mass tracking and determination of the weight threshold for living cells

Single cell mass measurements were performed using the original Q-PHASE software, which provides dry cell mass and motility (cell centroid movement between frames) data for individual cells. The initial distribution of A2780 cell masses was log-normal, with a range of 130–500 pg. Most of the cells had dry mass $\geq$130 pg and $\leq$400 pg, only small fraction was larger with dry masses higher than 500 pg. At the time 0, all tracked cells in the population were alive (verified visually by coherence-controlled holographic microscopy), with cell dry mass $>$130 pg. Consequently, we determined the cell mass threshold of viable A2780 cells as 130 pg. Similarly, we determined viable PC-3 cells with threshold 250 pg, but no dead cells were observed.

Cell-phosphorus colocalization measurement

For the colocalization of BP particles and cells, the novel method based on the merging of phase and amplitude imaging was used. This method combines quantitative phase imaging of weakly scattering or absorbing objects (cells) with the reconstructed amplitude imaging (similar to the bright field microscopy) of amplitude objects (BP or metal particles) recalculated from the hologram. Phosphorus accumulation was analysed using MATLAB custom script. Cells were segmented by thresholding of quantitative phase image (threshold 0.07 pg μm^{-1}) followed by removing of small objects and holes ($<$100 px). Similarly, BP particles were segmented by thresholding of amplitude image (threshold 3000). Overlay of cells and phosphorus areas was used for computation of the amount of accumulated phosphorus, which was determined as percent of the area of the cells (foreground) covered by the phosphorus. Moreover, phosphorus above/under the cells were also considered, thus percentage of background (outside cells) covered area was subtracted as correction and average of 5 field of views were computed for every sample. The disadvantage of this approach is that we are not able to quantify the amount of phosphorus in volume units or concentration, but we can analyse an increase in its amount in the cells.

Acknowledgements

This work was supported in part by grants from the Czech Science Foundation (18-24089S and 17-11456S). Z.S. and D.B. were supported by specific university research (MSMT No. 20-SVV/2018). M.F. was supported also by Grant Agency of Masaryk University (MUNI/A/1157/2017). This work was supported by the project Advanced Functional Nanorobots (reg. No. CZ.02.1.01/0.0/0.0/15_003/0000444 financed by the EFRR). Further, we would like to acknowledge Dr. Petr Beneš and Tereza Kučírková from the Faculty of Science, Masaryk University for their kind help with the flow cytometry measurement.

Conflict of interest

The authors declare no conflict of interest.

Keywords: 2D nanomaterials · black phosphorus · cytotoxicity · holographic microscopy · interference · nanoparticles · viability

[1] F. Feng, J. C. Wu, C. Z. Wu, Y. Xie, *Small* **2015**, *11*, 654–666; S. Bai, Y. J. Xiong, *Sci. Adv. Mater.* **2015**, *7*, 2168–2181.
[2] H. J. Yin, Z. Y. Tang, *Chem. Soc. Rev.* **2016**, *45*, 4873–4891.
[3] Z. P. Smith, B. D. Freeman, *Angew. Chem. Int. Ed.* **2014**, *53*, 10286–10288; *Angew. Chem.* **2014**, *126*, 10452–10454.
[4] P. Bollella, G. Fusco, C. Tortolini, G. Sanzo, G. Favero, L. Gorton, R. Antiochia, *Biosens. Bioelectron.* **2017**, *89*, 152–166.
[5] G. H. Yang, C. Z. Zhu, D. Du, J. J. Zhu, Y. H. Lin, *Nanoscale* **2015**, *7*, 14217–14231; X. R. Gan, H. M. Zhao, X. Quan, *Biosens. Bioelectron.* **2017**, *89*, 56–71.
[6] M. Fojtu, X. Y. Chia, Z. Sofer, M. Masarik, M. Pumera, *Adv. Funct. Mater.* **2017**, *27*, 7.
[7] a) W. Tao, X. B. Zhu, X. H. Yu, X. W. Zeng, Q. L. Xiao, X. D. Zhang, X. Y. Ji, X. S. Wang, J. J. Shi, H. Zhang, L. Mei, *Adv. Mater.* **2017**, *29*, 10; b) X. B. Zhu, X. Y. Ji, N. Kong, Y. H. Chen, M. Mahmoudi, X. D. Xu, L. Ding, W. Tao, T. Cai, Y. J. Li, T. Gan, A. Barrett, Z. Bharwani, H. B. Chen, O. C. Farokhzad, *ACS Nano* **2018**, *12*, 2922–2938; c) S. G. Wang, Y. Chen, X. Li, W. Gao, L. L. Zhang, J. Liu, Y. Y. Zheng, H. R. Chen, J. L. Shi, *Advanced Materials* **2015**, *27*, 7117–7122; d) X. Y. Yang, X. Y. Zhang, Z. F. Liu, Y. F. Ma, Y. Huang, Y. Chen, *J. Phys. Chem. C* **2008**, *112*, 17554–17558; e) J. Q. Liu, L. Cui, D. Losic, *Acta Biomater.* **2013**, *9*, 9243–9257; f) N. S. Gao, J. P. Nie, H. F. Wang, C. Y. Xing, L. Mei, W. Xiong, X. W. Zeng, Z. C. Peng, *J. Biomed. Nanotechnol.* **2018**, *14*, 1883–1897.
[8] a) L. Cheng, C. Wang, L. Z. Feng, K. Yang, Z. Liu, *Chem. Rev.* **2014**, *114*, 10869–10939; b) C. X. Sun, L. Wen, J. F. Zeng, Y. Wang, Q. Sun, L. J. Deng, C. J. Zhao, Z. Li, *Biomaterials* **2016**, *91*, 81–89; c) Z. B. Sun, H. H. Xie, S. Y. Tang, X. F. Yu, Z. N. Guo, J. D. Shao, H. Zhang, H. Huang, H. Y. Wang, P. K. Chu, *Angew. Chem. Int. Ed.* **2015**, *54*, 11526–11530; *Angew. Chem.* **2015**, *127*, 11688–11692; d) Y. T. Zhao, L. P. Tong, Z. B. Li, N. Yang, H. D. Fu, L. Wu, H. D. Cui, W. H. Zhou, J. H. Wang, H. Y. Wang, P. K. Chu, X. F. Yu, *Chem. Mater.* **2017**, *29*, 7131–7139; e) H. Li, C. Soria, F. Griscelli, P. Opolon, J. Soria, P. Yeh, C. Legrand, J. P. Vannier, D. Belin, M. Perricaudet, H. Lu, *Human Gene Ther.* **2005**, *16*, 1157–1167; f) H. Wang, X. Z. Yang, W. Shao, S. C. Chen, J. F. Xie, X. D. Zhang, J. Wang, Y. Xie, *J. Am. Chem. Soc.* **2015**, *137*, 11376–11382; g) J. D. Shao, H. H. Xie, H. Huang, Z. B. Li, Z. B. Sun, Y. H. Xu, Q. L. Xiao, X. F. Yu, Y. T. Zhao, H. Zhang, H. Y. Wang, P. K. Chu, *Nat. Commun.* **2016**, *7*, 13.
[9] a) Z. Z. Feng, X. M. Liu, L. Tan, Z. D. Cui, X. J. Yang, Z. Y. Li, Y. F. Zheng, K. W. K. Yeung, S. L. Wu, *Small* **2018**, *14*, 16; b) X. Z. Xie, C. Y. Mao, X. M. Liu, Y. Z. Zhang, Z. D. Cui, X. J. Yang, K. W. K. Yeung, H. B. Pan, P. K. Chu, S. L. Wu, *ACS Appl. Mater. Interfaces* **2017**, *9*, 26417–26428; c) X. Z. Xie, C. Y. Mao, X. M. Liu, L. Tan, Z. D. Cui, X. J. Yang, S. L. Zhu, Z. Y. Li, X. B. Yuan, Y. F. Zheng, K. W. K. Yeung, P. K. Chu, S. L. Wu, *ACS Cent. Sci.* **2018**, *4*, 724–738; d) C. Y. Mao, Y. M. Xiang, X. M. Liu, Z. D. Cui, X. J. Yang, Z. Y. Li, S. L. Zhu, Y. F. Zheng, K. W. K. Yeung, S. L. Wu, *ACS Nano* **2018**, *12*, 1747–1759.
[10] L. Tan, J. Li, X. M. Liu, Z. D. Cui, X. J. Yang, K. W. K. Yeung, H. B. Pan, Y. F. Zheng, X. B. Wang, S. L. Wu, *Small* **2018**, *14*, 11.
[11] D. Y. Wang, W. Zhao, *Abstr. Pap. Am. Chem. Soc.* **2015**, *249*, 1.
[12] S. Sajjad, S. A. K. Leghari, A. Iqbal, *ACS Appl. Mater. Interfaces* **2017**, *9*, 43393–43414.

[13] a) W. Yang, L. Gan, H. Q. Li, T. Y. Zhai, *Inorg. Chem. Front.* **2016**, *3*, 433 – 451; b) R. Gusmão, Z. Sofer, M. Pumera, *Angew. Chem. Int. Ed.* **2017**, *56*, 8052; *Angew. Chem.* **2017**, *129*, 8164.

[14] H. Liu, Y. C. Du, Y. X. Deng, P. D. Ye, *Chem. Soc. Rev.* **2015**, *44*, 2732 – 2743; D. Y. Zhang, L. Gan, Y. Cao, Q. Wang, L. M. Qi, X. F. Guo, *Adv. Mater.* **2012**, *24*, 2715 – 2720.

[15] a) Y. T. Yew, Z. Sofer, C. C. Mayorga-Martinez, M. Pumer, *Mater. Chem. Front.* **2017**, *1*, 1130 – 1136; b) M. Qiu, Z. T. Sun, D. K. Sang, X. G. Han, H. Zhang, C. M. Niu, *Nanoscale* **2017**, *9*, 13384 – 13403; c) M. B. Erande, M. S. Pawar, D. J. Late, *ACS Appl. Mater. Interfaces* **2016**, *8*, 11548 – 11556; d) A. N. Cao, Z. Liu, S. S. Chu, M. H. Wu, Z. M. Ye, Z. W. Cai, Y. L. Chang, S. F. Wang, Q. H. Gong, Y. F. Liu, *Adv. Mater.* **2010**, *22*, 103; e) A. Ambrosi, Z. Sofer, M. Pumera, *Angew. Chem. Int. Ed.* **2017**, *56*, 10443; *Angew. Chem.* **2017**, *129*, 10579 f) D. Li, A. E. D. R. Castillo, H. Jussila, G. Ye, Z. Ren, J. Bai, X. Chen, H. Lipsanen, Z. Sun, F. Bonaccorso, *Appl. Mater. Today* **2016**, *4*, 17; g) Z. Sofer, D. Sedmidubsky, S. Huber, J. Luxa, D. Bousa, C. Boothroyd, M. Pumera, *Angew. Chem. Int. Ed.* **2016**, *55*, 3382; *Angew. Chem.* **2016**, *128*, 3443; h) C. C. Mayorga-Martinez, Z. Sofer, M. Pumera, *Angew. Chem. Int. Ed.* **2015**, *54*, 14317; *Angew. Chem.* **2015**, *127*, 14525.

[16] a) Y. C. Du, H. Liu, Y. X. Deng, P. D. Ye, *ACS Nano* **2014**, *8*, 10035 – 10042; b) J. Plutnar, Z. Sofer, M. Pumera, *ACS Nano* **2018**, *12*, 8390; c) N. M. Latiff, W. Z. Teo, Z. Sofer, A. C. Fisher, M. Pumera, *Chem. Eur. J.* **2015**, *21*, 13991 ; d) N. M. Latiff, C. C. Mayorga-Martinez, Z. Sofer, A. C. Fisher, M. Pumera, *Appl. Mater. Today* **2018**, *13*, 310.

[17] X. L. Han, R. Gelein, N. Corson, P. Wade-Mercer, J. K. Jiang, P. Biswas, J. N. Finkelstein, A. Elder, G. Oberdorster, *Toxicology* **2011**, *287*, 99 – 104; L. Belyanskaya, P. Manser, P. Spohn, A. Bruinink, P. Wick, *Carbon* **2007**, *45*, 2643 – 2648; J. M. Wörle-Knirsch, K. Pulskamp, H. F. Krug, *Nano Lett.* **2006**, *6*, 1261 – 1268; A. Casey, E. Herzog, M. Davoren, F. M. Lyng, H. J. Byrne, G. Chambers, *Carbon* **2007**, *45*, 1425 – 1432.

[18] R. Parboosing, G. Mzobe, L. Chonco, I. Moodley, *Med. Chem.* **2017**, *13*, 13 – 21.

[19] N. Latiff, W. Z. Teo, Z. Sofer, S. Huber, A. C. Fisher, M. Pumera, *RSC Adv.* **2015**, *5*, 67485 – 67492; A. Kroll, M. H. Pillukat, D. Hahn, J. Schnekenburger, *Eur. J. Pharm. Biopharm.* **2009**, *72*, 370 – 377.

[20] G. Diaz, M. Melis, A. Musinu, M. Piludu, M. Piras, A. M. Falchi, *Eur. J. Histochem.* **2007**, *51*, 213 – 218; Y. B. Liu, D. A. Peterson, H. Kimura, D. Schubert, *J. Neurochem.* **1997**, *69*, 581 – 593.

[21] M. V. Berridge, A. S. Tan, *Arch. Biochem. Biophys.* **1993**, *303*, 474 – 482.

[22] A. A. Stepanenko, V. V. Dmitrenko, *Gene* **2015**, *574*, 193 – 203.

[23] J. O'Brien, I. Wilson, T. Orton, F. Pognan, *Eur. J. Biochem.* **2000**, *267*, 5421 – 5426.

[24] G. Fotakis, J. A. Timbrell, *Toxicol. Lett.* **2006**, *160*, 171 – 177.

[25] T. L. Riss, R. A. Moravec, A. L. Niles in *Mammalian Cell Viability: Methods and Protocols, Vol. 740* (Ed.: M. J. Stoddart), Humana, Totowa, **2011**, pp. 103 – 114.

[26] Z. Sofer, D. Bousa, J. Luxa, V. Mazanek, M. Pumera, *Chem. Commun.* **2016**, *52*, 1563 – 1566.

[27] P. Scherrer in *Bestimmung der inneren Struktur und der Größe von Kolloidteilchen mittels Röntgenstrahlen, Vol. 2,* Springer, Berlin, Heidelberg, **1918**, pp. 98.

[28] S. Das, S. Singh, V. Singh, D. Joung, J. M. Dowding, D. Reid, J. Anderson, L. Zhai, S. I. Khondaker, W. T. Self, S. Seal, *Part. Part. Syst. Charact.* **2013**, *30*, 148 – 157; Y. L. Chang, S. T. Yang, J. H. Liu, E. Dong, Y. W. Wang, A. N. Cao, Y. F. Liu, H. F. Wang, *Toxicol. Lett.* **2011**, *200*, 201 – 210.

[29] H. J. Heipieper, F. J. Weber, J. Sikkema, H. Keweloh, J. A. M. Debont, *Trends Biotechnol.* **1994**, *12*, 409 – 415.

[30] S. J. Song, Y. C. Shin, H. U. Lee, B. Kim, D. W. Han, D. Lim, *Nanomaterials* **2018**, *8*, 10.

[31] M. Rayamajhi, Y. Zhang, E. Miao in *The Inflammasome: Methods and Protocols, Vol. 1040*, Humana, Totowa, **2013**, pp. 85 – 90.

[32] U. T. Shankavaram, S. Varma, D. Kane, M. Sunshine, K. K. Chary, W. C. Reinhold, Y. Pommier, J. N. Weinstein, *BMC Genomics* **2009**, *10*, 277; W. C. Reinhold, M. Sunshine, H. F. Liu, S. Varma, K. W. Kohn, J. Morris, J. Doroshow, Y. Pommier, *Cancer Res.* **2012**, *72*, 3499 – 3511.

[33] M. Maes, T. Vanhaecke, B. Cogliati, S. C. Yanguas, J. Willebrords, V. Rogiers, M. Vinken in *Protocols in In vitro Hepatocyte Research, Vol. 1250* Eds.: M. Vinken, V. Rogiers), Humana, Totowa, **2015**, pp. 349 – 361.

[34] T. A. Zangle, M. A. Teitell, *Nat. Methods* **2014**, *11*, 1221 – 1228.

[35] J. A. Prescher, C. R. Bertozzi, *Nat. Chem. Biol.* **2005**, *1*, 13 – 21; R. Wayne, *Light and Video Microscopy*, Academic Press, Burlington, **2008**.

[36] B. Gál, M. Vesely, J. Collakova, M. Nekulova, V. Juzova, R. Chmelik, P. Vesely, *PLoS One* **2017**, *12*(8): e0183399.

Manuscript received: August 30, 2018
Version of record online: December 13, 2018